Theor Chem Acc (2009) 123:365–373
DOI 10.1007/s00214-009-0563-7

OVERVIEW

An overview of the electronic structure in trigonal bipyramidal clusters of main elements or mixed with transition metals

Carlo Mealli · Abdelatif Messaoudi · Andrea Ienco

Received: 9 December 2008 / Accepted: 24 March 2009 / Published online: 11 April 2009

Abstract Equatorial/apical bond repartitioning in TBP clusters, formed by main group elements only (e.g., $B_5H_5^{2-}$, $B_3H_3N_2$, etc.) or mixed with metal atoms (e.g., $[(L_2M)_3S_2]^n$, $[(L_3M)_3S_2]^n$, $[(CpM)_3S_2]^n$), is critically analyzed from the horizontal comparison of the experimental structures and in terms of basic MO concepts. The ideas are double-checked through specific DFT calculations or existing ab initio results. Based on the Wade's rules for *closo*-clusters, the five vertices systems are normally characterized by six skeletal electron pairs. In the main group clusters, the electron delocalization at the equatorial edges depends on the electronegativity of the apical groups and for the B_{eq}–B_{eq} bonds an inverse relationship between bond strength and bond length is remarked. In $[(L_2M)_3S_2]^n$ compounds with a total electron count (TEC) of 48, the six bonding electron pairs localize at the apical M–S bonds. In $[(L_3M)_3S_2]^n$ or $[(CpM)_3S_2]^n$, also with TEC = 48, the effective atomic number rule predicts three single M–M single bonds besides the six M–S apical ones. In actuality, only partial M–M bonding can be considered due to the intermediation of the capping sulphur atoms, that help shifting the antibonding character of populated *radial* levels with that of the vacant *tangential* ones (bonding). The qualitative MO arguments are supported by the topological nature of the calculated DFT wave functions. Moreover, the MO nature of three lowest LUMOs for $48e^-$ species help to rationalize experimental structural trends observed for the addition of up to five electrons.

1 Introduction

In 1982, Oriano Salvetti became the *pro-tempore* director of our institute. An earlier stay by one of us with Roald Hoffmann had stimulated our interest in MO theory and it was fortunate to be able to discuss with a physical chemist the most up to date quantum-mechanical methodologies, to which Salvetti was a successful contributor. An important conceptual difference emerged, namely that between *reductionism*, i.e. the adoption of always deeper theories to analyze a specific phenomenon (this point that has been also recently emphasized [1]) and a more generalized MO approach to the comparison of much chemical data [2]. Nowadays, the computational simulation of chemical reality has become truly adequate, also in the transition metal field [3, 4], and about every microscopic property of a molecule can be reliably calculated. However, it is not always true that good simulation is the equivalent of good understanding. Calculations yield precise numbers, but understanding resides in knowing the physical factors, that contribute to making up an observable, and being able to make qualitative order-of-magnitude estimates of the contributions of important factors. Such reasoning is most important for hands-on chemists, who look for the theoretical essence of a problem and wish theory to provide useful chemical guidance to the improvement of a process.

Dedicated to the memory of Professor Oriano Salvetti and published as part of the Salvetti Memorial Issue.

Electronic supplementary material The online version of this article (doi:10.1007/s00214-009-0563-7) contains supplementary material, which is available to authorized users.

C. Mealli (✉) · A. Messaoudi · A. Ienco
Istituto di Chimica dei Composti Organometallici,
ICCOM-CNR, Via Madonna del Piano 10,
50019 Sesto Fiorentino (Florence), Italy
e-mail: mealli@iccom.cnr.it

There is much chemical information in wave functions that an appropriate topological analysis may extract. Fragment orbital analysis has been always considered a valid interpretational tool at various levels of theory, from the earlier attempts to adapt it to HF calculations [5] to the description available in the ADF package [6–8], of the multi-electronic DFT wave functions in terms of selected fragment orbitals. Also the approximate wave functions from ehmo (extended Hueckel molecular orbital) calculations (not containing explicitly electron correlation) have played a basic role for providing most simple interaction diagrams, which are a source of readily accessible information for synthetic and mechanistic chemists. This analytical method has the advantage of being extremely portable (for example the CACAO package [9, 10] that anyone can use) and productive (it helps to predict chemical behaviour and design experiments). Obviously, artefacts are possible at a low computational level, and it is therefore necessary to rely continually on experimental validation as well as on the support of the best calculations possible in the trade. That the latter are nowadays affordable does not vitiate the advantages of a qualitative analysis. Just as an example, the simplest MO picture of a dimeric $Pt_2(\mu\text{–}S)_2$ complex, reported to have very short Pt–S and S…S distances [11], had illogical aspects [12]. A significant improvement was made after tentatively replacing the S bridges with hydroxo groups, and these results were also supported by DFT calculations. Eventually, repetition of the experiments confirmed that our hypothesis was indeed correct.

By pursuing the combined MO strategy outlined, we now analyze a wide class of trigonal-bypiramidal (TBP) compounds formed by main group elements or mixed with transition metals. Horizontal comparisons between many experimental structures allow developing general MO arguments, which have been constantly double-checked with computations at the higher level (ours or by others). Our focus is on the relations between bonding at the TBP axial and equatorial edges, and in some case also between the apexes. The point is exemplified in Scheme 1 for the simplest *closo*-cluster $B_5H_5^{2-}$ with six bonding electron pairs (Wade's rules [13–15]) and concerns the relations between the *classical* description of the bonding (six apically localized $2e^-/2c$ bonds in **1a**) and the alternative *non-classical* one (**1b**) where bonding partially extends to the equatorial edges.

In this light, we also consider TBP metal analogues with M_3S_2 skeleton, some of which exhibit the *non-classical* picture **1b** with equatorial M–M bonding, while others have only localized M–S bonds. The MO picture individuates the affecting parameters, in particular, the total electron count (TEC) of the cluster and the number of terminal ligands. Also, significant correlations are made between the various species including the possible origin of the distortion from the skeletal D_{3h} symmetry when TEC > 48.

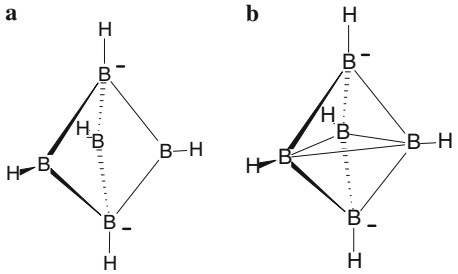

Scheme 1 Classical (**a**) vs. non-classical (**b**) bonding description for $B_5H_5^{2-}$

2 Discussion

2.1 General considerations

As inorganic chemists, our interest for TBP clusters was stimulated by the complex $[(L_2Cu)_3S_2]^{3+}$, **1**, (L_2 = uncharged dinitrogen chelate) [16, 17], for which we suggested, besides skeletal bonding, also a *trans*–axial one between S atoms, in spite of their large separation 2.7 Å [18].

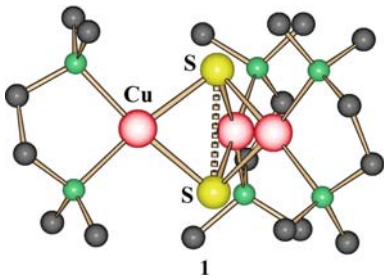

1

The proposal followed the experimental observation that in the tetranuclear compounds $[\{M_2(\eta^5\text{–}C_5Me_5)_2(\mu\text{–}CH_2)_2\}_2(\mu\text{–}S_4)]^{2+}$ (M = Rh, Ir) (Scheme 2) [19, 20] half S–S bonds at distances of 2.7–2.9 Å exist thanks to the oxidative coupling between the disulphide ligands of the dinuclear precursors [21]. Therefore, we thought that also the two S^{2-} ions in **1** may be coupled thanks to an inner electron transferring to the metals. The proposal has raised a fierce theoretical debate [22].

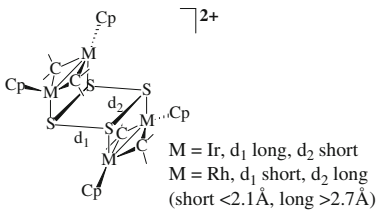

Scheme 2 S_4^{2-} rings with S–S half bonds

As mentioned, a good reference point also for TBP metal systems is the electronic structure of *closo*-clusters of $B_5H_5^{2-}$ and with the effects induced by heteronuclear apical groups such as CH, SiH, N or P. The distribution of bonding in these species has already received great theoretical attention [23–33]. One of the most reliable MP2 optimized structure of $B_5H_5^{2-}$ [23] has B_{ax}–B_{eq} distances of 1.684 Å and longer B_{eq}–B_{eq} ones (1.811 Å). It is reported that the latter value is shortened when apical N atoms are present (1.759 Å) but significant lengthening (2.078 Å) is induced by the SiH groups. Similar trends were found from another MP2 study [24] although the optimized distances are all somewhat shorter. Apparently, these trends suggest that the *non-classical* picture **1b** with more equatorial bonding can be favoured by more electronegative apical elements. The point has received much attention through precise structural determinations [32], electron density measurements [33] and various qualitative and ab initio approaches [23–31]. From a series of derived parameters such as the aromatic stabilization energy (ASE), the Wiberg indexes (WI), the natural atomic orbitals bond orders (NAO) and the nuclear independent chemical shifts (NICS), von Raguè Schleyer et al. [23] conclude that delocalization is a realistic feature, but the effect of the apical substitution is opposite to the apparent one. In particular $B_3H_3N_2$ has small B_{eq}–B_{eq} bonding although the corresponding separations are the shortest. This result is opposite to that of Burdett and Eisenstein [24] who calculated that only $B_3H_3N_2$ presents a small positive B_{eq}–B_{eq} overlap population whereas the values are negative for all the other derivatives. In the next section, we will outline a simple qualitative picture of the overall MO architecture that helps clarifying the controversial aspects of the problem.

Back to the TBP metal compounds, the apical/equatorial bond repartitioning is also intriguing. We have previously considered M_2P_3 skeletons with apical metal atoms [34], but here we limit ourselves to *closo*-M_3S_2 clusters which present a rich variety of electronic situations. In fact, although the Wade's rules [13–15] are in principle still applicable, the TEC is highly variable in these compounds and it certainly affects the presence or absence of the equatorial M–M bonding that is likely within the limits of the delocalized/localized pictures of Scheme 1.

A search in the Cambridge database[1] provided about 300 homo- or hetero-metallic M_3S_2 compounds, which differ for the number of terminal ligands besides the TEC. We limited their number by considering only homometallic species of formulae $[(L_2M)_3S_2]^n$, $[(L_3M)_3S_2]^n$ or $[(CpM)_3S_2]^n$. Essentially, the TEC varies between 47 and 53, but D_{3h} skeletal symmetry is found only for TEC = 48, independently from the nature and number of terminal ligands. In the $[(L_2M)_3S_2]^n$ systems with square planar d^8 metals, no M–M bonding occurs. Conversely, pyramidal L_3M (or CpM) fragments ($M = d^6$) are attributed 16 valence electrons and, provided that each capping sulfido ion donates $2e^-$ to each metal atom, three M–M bonds are predicted by the effective atomic number rule (EAN).[2] Deviation from TEC = 48 should destroy the equivalence of the M–M interactions although there are some apparent contradictions.

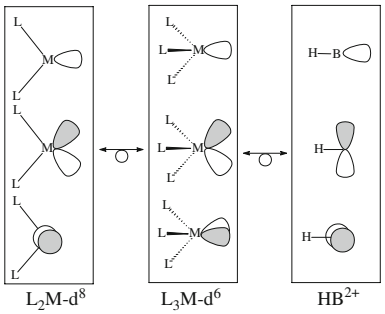

Scheme 3 Isolobality of the fragments at the five vertices of the TBP compounds

To correlate the electronic structure of the main group and metal TBP compounds, we exploit the concepts of the *isolobal* analogy [35] that can be formulated for BH^{2+}, L_2M–d^8 and L_3M–d^6 fragments (see Scheme 3). In all cases, the fragment molecular orbitals (FMOs) of the TBP equatorial groupings consist of one σ and two orthogonal π orbitals (either hybridized d_π or pure p). Considered vacant, these levels must compete to share part of the six bonding electron pairs, in principle provided by the apical groups (e.g., two sulfido dianions or the very formal BH^{4-} anions in $B_5H_5^{2-}$).

2.2 TBP clusters of main group elements

The principle of electroneutrality suggests that for $B_5H_5^{2-}$ the fragmentation $3BH^0 + 2BH^-$ can be better than the $3BH^{2+} + 2BH^{4-}$ one. In any case, the assignment of six electrons (all unpaired) to each fragment in the MO diagram of Fig. 1 is rather irrelevant, since the electron partitioning depends on the overall cluster and not on the fragments. Also consider that in $B_3H_3N_2$, the accumulation of negative charges at the apexes is not so illogic since the trend for the nitrogen atoms is to reach the octet N^{3-}. At the left side of the diagram, the orbital combinations of the three equatorial BH fragments (Scheme 3) are reported**.** The a_2'' and e'' FMOs (formed by perpendicular p boron orbitals) find appropriate

[1] Cambridge Structural Database System, Cambridge Crystallographic data Centre, 12 Union Road, Cambridge, CB2 1EZ, UK.

[2] The EAN rule predicts that the number of M–M bonds (n) is equal to the half difference between the highest electron configuration achievable by all the metals (in this case 3 × 18) and the actual number of valence electrons (=TEC). For $48e^-$ TBP compounds, $n = 3$.

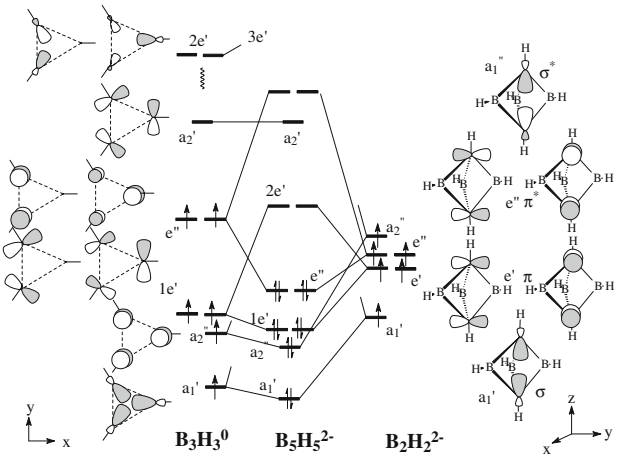

Fig. 1 A qualitative diagram for interaction in $B_5H_5^{2-}$ between selected FMOs of B_3H_3 (*left side*) and those of $B_2H_2^{2-}$ (*right side*)

symmetry partners at the two axial units (right side) to form three B_{eq}–B_{ax} localized bonds. To the other three B–B bonds (Scheme 1a) must concur the in-plane combinations a_1' and 2e′, formed by BH in-pointing σ hybrids, which are adequate to interact with the apical symmetry partners. Indeed, the total-symmetric a_1' MO of $B_5H_5^{2-}$ is strongly stabilized by the interaction and accounts for both B_{eq}–B_{ax} and B_{eq}–B_{eq} bonding.

The interaction $\langle 2e'|e'\rangle$ (Scheme 4a) is not very feasible, mainly because of the high energy of the σ antibonding equatorial FMOs 2e′. Instead, the boron axial p_x and p_y orbitals find a stronger match with the in-plane *tangential* orbitals 1e′ (see the top view in Scheme 4b). Similarly to a_1', the interaction $\langle 1e'|e'\rangle$ is not exclusively devoted to the fifth and sixth B_{eq}–B_{ax} σ bonds, but drifts electron density into B_{eq}–B_{eq} *tangential* bonding orbitals, hence contributes to an overall electron delocalization. Although experimental determinations of the electron density for the molecule $B_3C_2Et_5$ have not shown any B_{eq}–B_{eq} bond critical points [33], the indicated mechanism should favour the attraction between the B_{eq} atoms. In summary, these MO arguments support the *non-classical* picture **1b**. Also, the unusual 3D aromaticity computed for this systems [23] finds its justification in the population of the in-pointing MOs a_1' and 1e′ that are bonding for the overall TBP skeleton.

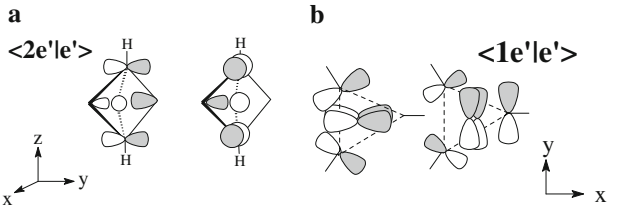

Scheme 4 e′-type combinations of the p_x and p_y orbitals at the apical atoms with **a** in-plane radial orbitals **b** with the tangential ones

Significant trends emerge also from the overlap populations provided by the simplest calculations. By using the geometry of the MP2 optimized $B_5H_5^{2-}$ model, the ehmo ROP values for B_{ax}–B_{eq} and B_{eq}–B_{eq} are 0.733 versus 0.271. Such a macroscopic difference, justified by the different number of orbital interactions, does not exclude significant B_{eq}–B_{eq} bonding. This is confirmed from an unbiased model with nine equal B–B edges (1.8 Å), that shows a reduced difference of the ROP values (0.67 vs. 0.37) with still larger B_{ax}–B_{eq} bonding. Correspondingly, a greater accumulation of negative charge at the axial atoms is noticed (-0.400 vs. -0.137 $e^-/Å^3$).

The MO trends also help clarifying what happens with more electronegative apical elements (nitrogen). In $B_3H_3N_2$, all the six axial FMOs are low in energy (hence the bonding electrons remain more localized at the apexes according to the electronegativity of the element). Therefore, there is a smaller flow of the electron density in the equatorial bonding levels, in particular the *tangential* FMOs 1e′ (Scheme 4b). For instance, the computed population of 1e′ dramatically drops from 73% in $B_5H_5^{2-}$ to 28% in $B_3H_3N_2$ and, simultaneously, the B_{eq}–B_{eq} ROP values almost vanishes (from 0.271 to 0.015). The result is fully consistent with the response of the MP2 calculations of von Raguè Schleyer et al. [23], in spite of the fact that the B_{eq}–B_{eq} distances are for $B_3H_3N_2$ the shortest in the series. Instead other calculations [24] predicted some B_{eq}–B_{eq} bond delocalization only for $B_3H_3N_2$, whereas there would be repulsive interaction in $B_3H_5Si_2$, which has indeed the longest B_{eq}–B_{eq} distance (2.078 Å). For us (but also in Ref. [23]), the compound instead features the second largest bond delocalization, as shown by the significantly positive ROP of 0.137.

The most interesting conclusion is that in these TBP compounds a classic paradigm of chemistry is broken, namely that of the direct correlation between bond length and bond strength. This uncommon situation is rare but we observed it also in some protonated M–M bond (M = Fe, Ru) [36], in which the transformation from a $2e^-$/2c bond to a $2e^-$/3c one, weakens the M–M interaction while the M–M distance is surprisingly shortened. Perhaps, this inverse relationship is at the origin of the controversial interpretation of bonding in the main group TBP molecule [23, 24].

2.3 Overview of TBP metal clusters with capping sulphur atoms

In TBP metal clusters, the relationship between axial and equatorial interactions directly affects M–M bonding, although this is clearly absent in the $48e^-$ complexes $[(L_2M)_3(\mu_3\text{–}S)_2]^n$, where the d^8 metal atoms are saturated in local square planar geometry. Amongst the latter, there

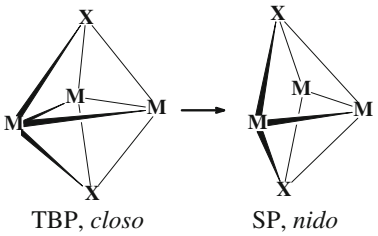

Scheme 5 Opening of one equatorial edge of the TBP cluster upon electron reduction

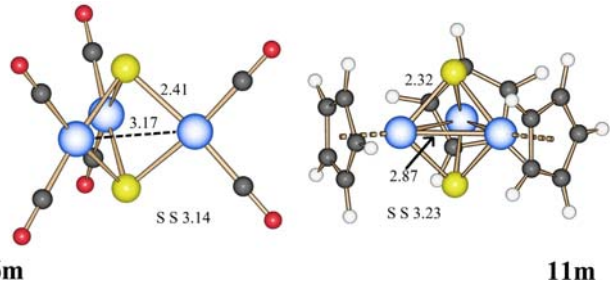

Fig. 2 The DFT optimized structures of the dication $[(CpRh)_3(\mu_3–S)_2]^{2+}$, **11m**, and the anion $[(CO)_2\ M)_3(\mu_3–S)_2]^{-}$, **6m**

are various nickel compounds ($[(L_2Ni)_3(\mu_3–S)_2]^{2+}$, **5** [37–43]) or species such as $[(CO)_2M)_3(\mu_3–S)_2]^{-}$, M = Rh, Ir; **6a** [44], **6b** [45, 46]. Two more electrons (TEC = 50) are only found in the mentioned copper species $[(L_2Cu)_3S_2]^{3+}$, **1**, with triplet ground state. The orbital underpinnings of the unique S…S coupling proposed in these latter compounds, have been already outlined [18, 22] and will summarized below.

Another important class of $48e^-$ TBP clusters features three ligands per metal, i.e. $[(L_3M)_3(\mu_3–S)_2]^n$. An example is $[(CO)_9Mn_3S_2]^-$, **7** [47, 48] with somewhat elongated Mn–Mn bonds (2.77 Å). A selenium analogue of **7** [49] exists in the dianionic form (TEC = 49) with an essentially broken Mn–Mn bond [50]. The transformation of the *closo*-TBP structure into a *nido*-square pyramidal one (Scheme 5) is magnified in $50e^-$ clusters such as $[(CO)_6(PPh_3)_3Fe_3S_2]$, **8** [51].

The three ligands of each metal can be replaced by one cyclopentadienyl ring (also variously substituted) and the $[(CpM)_3(\mu_3–S)_2]^n$ species have TEC in between 47 and 53. Only the reference $48e^-$ cluster $[(CpCo)_3(\mu_3–S)_2]^{2+}$, **10** [52] or its rhodium analogue $[(CpRh)_3(\mu_3–S)_2]^{2+}$ **11** [53] are undistorted, but TBP → SP rearrangements are observed for different TECs. Surprisingly, the rare $47e^-$ species $[(CpFe)_3(\mu_3–S)_2]^0$, **12**, experimentally shows equivalent Fe–Fe bonds, but in DFT calculations one bond Fe–Fe bond appears shorter than the others by 0.2 Å [54].

TECs > 48 are the product of electron reduction or involve electron richer metals. For instance, the whole series of derivatives of $[(CpCo)_3(\mu_3–S)_2]^{2+,1+,0}$, **10**, **13**, **14** is known [52], whereas nickel supports the $52e^-$ and $53e^-$ species $[(CpNi)_3(\mu_3–S)_2]^{1+,0}$, **15** and **16** [55]). No $51e^-$ complex is structurally characterized but the mono-anion $[(CpCo)_3(\mu_3–S)_2]^-$ is electrochemically obtainable [55]. Given the existence of these reduced derivatives, it is important for predicting behaviours to have qualitative information about the three LUMOs of the $48e^-$ prototype.

2.4 MO features of $[(L_2M)_3S_2]^n$ compounds

DFT optimizations for the Rh_3S_2 models $\mathbf{6_m}$ and $\mathbf{11_m}$ provide acceptable geometries. The Rh–Rh and Rh–S distances of the anion $[(CO)_2Rh)_3(\mu_3–S)_2]^-$, **6**, are given in Fig. 2 and are somewhat longer than the experimental values of 3.06 Å (ave.) and 2.35 Å (ave.), respectively.

An even better agreement is found in the dication $[(CpRh)_3(\mu_3–S)_2]^{2+}$, **11** [53], where the Rh–Rh distances are definitely shorter [2.83 Å (ave)] as well as the Rh–S distances [2.28 Å (ave)]. The S–S separations of 3.11 and 3.19 Å (in **6** and **11**, respectively) exclude any *trans*–axial coupling, being at least 0.4 Å larger than in **1**.

Much information can be extracted from the comparison of the interaction diagrams for **11** and **6** in Fig. 3. The FMOs of the equatorial $(CO)_2Rh$ or CpRh fragments appear at the right and left sides, respectively, and those of the capping S^{2-} ions in the centre. The latter are grouped according to the σ, π, π^* and σ^* symmetries, but correspond to those of the two apical BH^- groupings in $B_5H_5^{2-}$ (right side of Fig. 1), with the difference that the levels are low in energy and populated. Analogously to $B_3H_3N_2$, this situation could disfavour equatorial bonding, but this is not equally true for the metal compound (see below).

A confirmation of the different electronic structures of **6** and **11** can be obtained by fixing the same Rh_3S_2 skeleton in the different ligand environments (Rh–Rh = 3.0 Å, Rh–S = 2.32 Å and S–S = 3.10 Å). The corresponding ROP values suggest that Rh–Rh interactions are four times larger in **11** than in **6** (0.060 vs. 0.015). The residual M–M attraction in the latter is far from real bonding.

The diagram for $[(L_2M)_3S_2]^n$, at the right side of Fig. 3 highlights the donations from the sulfido dianions into empty frontier levels of the $L_2M–d^8$ fragments (see Scheme 3). Again those into the upright d_π hybrids a_2'' and e'' are responsible for three Rh–S bonds and a fourth one is of the a_1' type (overall bonding as in $B_5H_5^{2-}$). Importantly, the interaction of e′ type are particularly weak. The 3e′ metal levels (antibonding σ hybrids) lie too high in energy, but also the *tangential* 2e′ levels are high being pure p metal orbitals. Therefore the lack of significant electron transfer from the low S_2^{2-} π levels into the *tangential* metal combinations, excludes significant M–M bonding. Instead the electron was at the origin of the $B_{eq}–B_{eq}$

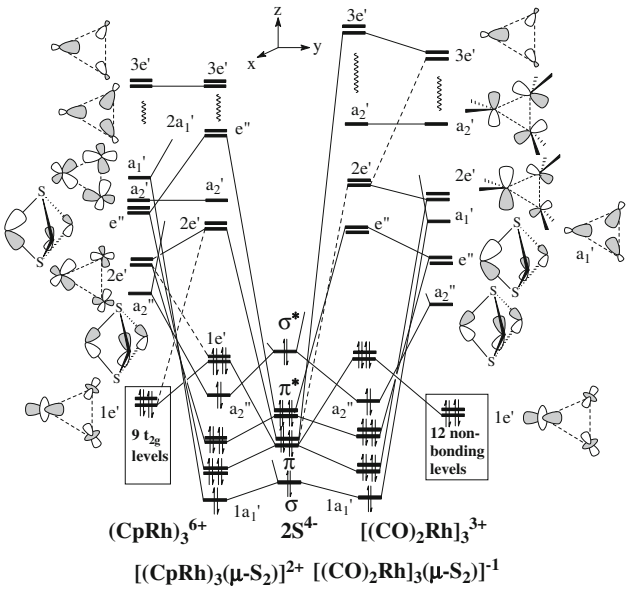

Fig. 3 Comparative MO diagrams for the interaction of two discrete sulphide anions (*centre*) with the trinuclear fragments $(CpRh)_3^{6+}$ (*left side*) and $[(CO)_2Rh]_3^-$ (*right side*)

bonding in $B_5H_5^{2-}$ (see Fig. 1). Because of the weak e′ interactions, also the Rh–S distances appear longer in **6m** than in **11m** (2.41 vs. 2.32 Å). In conclusion, the delocalization of six bonding electron pairs in the Rh_3S_2 core of $[(CO)_2Rh)_3(\mu_3\text{–}S)_2]^-$ is not very efficient.

The diagram for $[(L_2M)_3S_2]^n$ species (right side of Fig. 3) is also useful to revise the origin of the S–S coupling in the $50e^-$ complex $[(L_2Cu)_3S_2]^{3+}$, **1** [18, 22]. First, the two extra electrons occupy, unpaired, the e″ M–S antibonding levels (LUMOs of $48e^-$ complexes), hence cause further Cu–S bond weakening but no effect is expected for M–M bonding. Instead for the S–S coupling, a major role is played by the interactions of the a_2'' type. Scheme 6 shows that, for large S–S separations (>3 Å), the $2S^{2-}$ σ^* combination lies low in energy and normally donates two electrons to the d_π metal combination (black bars). However, copper d orbitals are amongst the lowest in energy amongst all metals and also their in-phase a_2'' combination lies particularly low, possibly below the S_2 σ^* partner even for a relatively long S…S distance.

If the order of the interacting levels can be reversed (empty bars in Scheme 6), the classic donation from the S_2^{2-} dianion can transform into a metal back-donation to S_2^{2-} σ^*. This implies that the oxidation concerns the discrete sulfido ions while a formal $2e^-$ reduction of the Cu_3 grouping has occurs ($2d^9d^8 \rightarrow 2d^9d^{10}$) [18, 22]. The point is numerically confirmed by the halved population of S–S σ^* level with respect to aforementioned $48e^-$ $[(L_2M)_3S_2]^n$ complexes.

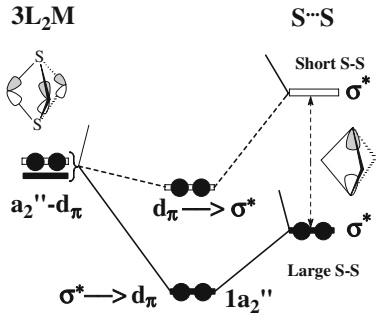

Scheme 6 The relative energy order of the a_2'' M_3 levels with respect to the S_2 σ^* one affects the sulphido/disulpido nature of the capping ligands

Interestingly, Alvarez and co-workers have reported DFT computational evidence [56] that the $48e^-$ TBP clusters of the type $[(L_2Ni)_3(\mu_3\text{–}S)_2]^{2+}$ can be oxidized to the tetra-cation $[(L_2Ni)_3(\mu_3\text{–}S)_2]^{4+}$ with the formation of a strong S–S *trans*–axial bond (2.25 Å). Evidently, the two electrons are removed from the bonding MO a_2'' that was engaged in the dative $S_2 \rightarrow Ni_3$ interaction (refer to the right side of Fig. 3 and Scheme 6). The level must be first promoted to become the HOMO and this seems possible even for a minor shrinking of the S–S separation, given its S_2 σ^* character. Then, the removal of two electrons from HOMO a_2'' can trigger the direct S–S bond at the expenses of the Ni–S ones (recall that the populated a_2'' MO was essentially M–S bonding). It is noteworthy that the vacation of the level does not completely destroy the Ni–S bonding. In fact, there are good indications that a low lying a_2'' combination formed by outpointing sulphur lone pairs (not shown in the diagram) can become a week donor toward the Ni_3 a_2'' empty partner. In this manner, the $2e^-$oxidation affects the sulphur atoms, while the TEC of 48 remains unchanged. A similar electronic situation, that determines bonding between the apexes of the TBP, seems to occur in C_5R_6 propellanes [57] and in the recently reported Ge_5R_6 analogues [58]. A finer comparison of the S–S coupling in both Cu_3S_2 and Ni_3S_2 frameworks will be given elsewhere [59].

2.5 MO features of $[(L_3M)_3S_2]^n$ and $[(CpM)_3S_2]^n$ compounds

The set of metal FMOs (left side of Fig. 3) for $[(CpRh)_3(\mu_3\text{–}S)_2]^{2+}$ include, beside the σ hybrids, in-plane and upright metal π orbitals, that are not separated in energy as much as in the case of the $[(CpRh)_3(\mu_3\text{–}S)_2]^{2+}$ complex. All the levels are empty for the formal d^6 metal configuration and in principle contribute to Rh–S and Rh–Rh bonding. The *isolobal analogy* of Scheme 6 may be applied and again three apical M–S bonds can be seen as due to a_2'' and e″ interactions as in $B_5H_5^{2-}$ and **6**.

Analogously, the a_1' bonding interaction is similarly delocalized over the whole TBP framework. Instead, the interactions of the e′ type are now more problematic. The *radial* σ metal hybrids 3e′ lie high in energy and hardly interact with the populated $2S^{2-}$ π set. The gap is lower with respect to the *tangential* metal combination 2e′ formed by the d_π orbitals is smaller but the overlap with π set of capping sulphur atoms is not sufficient to justify good M–M bonding through electron delocalization. On the other hand, EAN rule for $48e^-$ compounds of this sort predicts M–M bonds of order one and the corresponding experimental distances in **11** and other similar compounds, although somewhat long, are not in contrast with such a picture. The point is to find whether there is any evidence for nine instead of six (Wade's rules) bonding electron pairs in these clusters. The only possibility is that three of the populated "t_{2g}" non-bonding levels (shown in the box at the left side of Fig. 3) are instead involved in direct M–M bonding. This seems somewhat illogic since the 1e′ set of *radial* $x^2 - y^2$ atomic orbitals is antibonding and destabilized (HOMO within the box) while the *tangential* bonding set 2e′ is the vacant bonding LUMO. Only a switching of the respective characters could activate M–M single bonds. The unfavourable orbital order cannot be totally reversed but some mixing occurs (see the dashed lines in the MO interaction diagram) thanks to the intermediation of the lower S e′ levels. Partial inversion of the character between the MOs 1e′ and 2e′ is confirmed by the MO drawings of Fig. 4 (obtained from the actual DFT wave functions of **11m**). In fact, the selected HOMO show some Rh–Rh bonding character along y axis, whereas the LUMO is antibonding at the other two Rh–Rh vectors. This is an example of how the qualitative MO analysis can help interpreting the results of DFT calculations and extracting useful chemical information form them. Similarly to non-metallic TBP compounds, equatorial M_3 bonding arises here from orbital mixing and it is not substantiated from the clear presence of three bonding electron pairs. Eventually, the picture of these *closo*-metal clusters is intermediate between two conceptual limits, namely the EAN rule (nine edge-localized electron pairs) and the Wade's rule (six delocalized skeletal pairs).

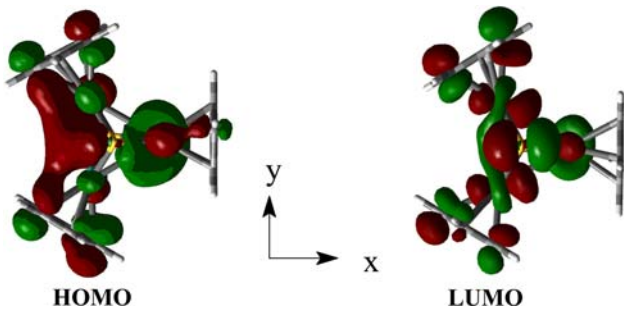

Fig. 4 Drawings (from DFT data) of a member of the 1e′ set (HOMO) and the corresponding 2e′ set (LUMO) for the model of $[(CpRh)_3(\mu_3\text{–}S)_2]^{2+}$, **11m**

The dichotomous bonding or antibonding nature of the 2e′ LUMOs of $48e^-$ $[(CpM)_3(\mu_3\text{–}S)_2]^n$ systems is important also to understand the behaviour of the redox derivatives and it has been amply debated in the past [55, 60, 61]. In fact up to five electrons may be added to the system, thus, beside the MOs 2e′, also the subsequent a_2' level (the strongly M_3 antibonding LUMO + 2 in Fig. 3) may be involved in the redox process. Population of the latter is not necessarily restricted to the $53e^-$ cluster $[(CpNi)_3(\mu_3\text{–}S)_2]^0$ [55] as the relatively small energy gap between 2e′ and a_2' can involve the latter level in Jahn-Teller effects also for the lower TECs[3] and induce the TBP → SQ deformation (Scheme 5).

Without examining here the various structural effects occurring with the population of the higher MOs, we just mention the dichotomy of the spin pairing/unpairing in some $50e^-$ compounds. For instance, $[(CpCo)_3(\mu_3\text{–}S)_2]^0$ [52] or its selenium analogue [62] are proved to exist as spin isomers. The triplet structure is symmetric D_{3h} [52, 63] and has probable configuration $(2e')^2$, whereas the diamagnetic isomer clearly distorts from TBP to SP geometry (Scheme 4) thanks to the JT effect mixing $2a_2'$ and one member of 2e′. In this manner, the two highest paired electrons populate one M–M antibonding level, hence one of the three equatorial bonds is broken. The deformation effects in the nickel compounds $[(CpNi)_3(\mu_3\text{–}S)_2]^{1+,0}$, with 52 and 53 electrons, have been also amply discussed [55] and appear consistent with the present overall MO picture that assigns M–M antibonding character also to the LUMOs 2e′ in spite of their presumable *tangential* bonding character (see Fig. 4).

2.6 Closing remarks

Skeletal bonding trends in TBP compounds of main group elements and analogous metal complexes have been compared based on the *isolobal analogy* of their FMOs. The qualitative analysis is consistent with the accurate results of the most accurate MP2 calculations available for main group molecules [23] and provides an MO support to interpret the distribution of bonding. Also, it helps to dismiss some inconsistent conclusion from different ab initio studies [24]. As an interesting remark, a reverse trend between bond strength and length emerges for the equatorial B–B bonds on B_3X_2 skeletons with respect to paradigmatic chemical assumptions.

The paper also reviews the known prototypes of the TPB M_3S_2 clusters and correlates them with the main group

[3] To justify some experimental data it has been assumed that a_2' may even be lower than 2e′ [55].

analogues from the MO viewpoint. It is found that, in $48e^-$ $[(L_2M)_3S_2]^n$ compounds, six skeletal electron pairs remain largely localized at the apical M–S bonds and equatorial M–M bonding is safely excluded (axial bond localization). The picture is also exploited to account for a more or less pronounced *trans*–axial S–S coupling in the Ni_3S_2 and Cu_3S_2 clusters, with TEC of 46 and 50, respectively.

The $[(L_3M)_3S_2]^n$ or $[(CpM)_3S_2]^n$ compounds with 48 valence electrons and d^6 metal centres, for which the EAN rule predicts three M–M bonds (hence nine bonding electron pairs localized at the TBP edges), are examined. The MO picture shows that M–M bonding is not so straightforward but it partially occurs only thanks to the intermediation of the capping S ligands. These contribute to a mechanism that favours electron delocalization at the M–M equatorial edges whereas it is difficult to figure out nine electron pairs dedicated to skeletal bonding. The mechanism of the bond delocalization is, however, somewhat different from that in TBP main group *closo*-clusters, as the capping S atoms favour the mixing of populated metal d orbitals, usually considered non-bonding. Finally, the same MO picture is exploited to interpret some of the known structural effects occurring when the TECs of $[(CpM)_3S_2]^n$ compounds varies from 48 to 53.

2.7 Computational details

Structural optimizations were performed by using the Gaussian03 suite of programs [64]. The Becke's three-parameter hybrid exchange-correlation functional [65], with the nonlocal gradient correction of Lee et al. [66] (B3LYP), was used. Frequencies were calculate the optimized structures as minima. The Stuttgart/Dresden effective core potential was used for metals [67], and the basis set 6–31G(d, p) [68] for the other atoms. The coordinates of the optimized structures are provided as Supplementary information to the paper.

Acknowledgments Thanks are expressed to Professor Roald Hoffmann for comments and suggestions. The work was carried out under the Project No. 7 of the DPM at CNR. Computations have performed thanks to the time allotted by CINECA and CASPUR under the agreement with CNR.

References

1. Bencini A (2008) Inorg Chim Acta 361:3820. doi:10.1016/j.ica.2008.03.076
2. Hoffmann R (1998) Theochem 424:1. doi:10.1016/S0166-1280(97)00219-4
3. Improta R, Barone V, Santoro F (2007) Angew Chem Int Ed 46:405–408. doi:10.1002/anie.200602907
4. Barone V, Improta R, Rega N (2008) Acc Chem Res 41:605. doi:10.1021/ar7002144
5. Colle R, Fortunelli A, Re N, Salvetti O (1988) J Am Chem Soc 110:8016. doi:10.1021/ja00232a010
6. ADF2008 01; SCM, Theoretical Chemistry, Vrije Universiteit, Amsterdam. Available at http://www.scm.com
7. Te Velde G, Bickelhaupt FM, van Gisbergen SJA, Fonseca Guerra C, Baerends EJ, Snijders JG, Ziegler TJ (2001) Comput Chem 22:931
8. Fonseca Guerra C, Snijders JG, Te Velde G, Baerends EJ (1998) Theor Chem Acc 99:391
9. Mealli C, Proserpio DM (1990) J Chem Ed 67:399
10. Mealli C, Ienco A, Proserpio DM (1998) Book of Abstracts of the XXXIII ICCC, ICCC, Florence, Italy, p 510
11. Li H, Carpenter GB, Sweigart DA (2000) Organometallics 19:1823. doi:10.1021/om000100d
12. Ienco A, Caporali M, Zanobini F, Mealli C (2009) Inorg Chem 48 (in press). doi:10.1021/ic8023748
13. Wade K (1971) J Chem Soc Chem Commun 792
14. Wade K (1976) Adv Inorg Radiochem 18:1
15. O'Neill ME, Wade K (1982) Comprehensive organometallic chemistry. In: Wilkinson G, Stone FGA, Abel E (eds) Pergamon Press, New York
16. Brown EC, York TJ, Antholine WE, Ruiz E, Alvarez S, Tolman WB (2005) J Am Chem Soc 127:13752. doi:10.1021/ja053971t
17. York JT, Bar-Nahum I, Tolman WB (2007) Inorg Chem 46:8105. doi:10.1021/ic700760p
18. Mealli C, Ienco A, Poduska A, Hoffmann R (2008) Angew Chem Int Ed 47:2864. doi:10.1002/anie.200705296
19. Isobe K, Ozawa Y, Vázquez de Miguel A, Zhu TW, Zhao KM, Nishioka T, Ogura T, Kitagawa T (1994) Angew Chem Int Ed Engl 33:1882. doi:10.1002/anie.199418821
20. Nishioka T, Kitayama H, Breedlove BK, Shiomi K, Kinoshita I, Isobe K (2004) Inorg Chem 43:5688. doi:10.1021/ic049855t
21. Poduska A, Hoffmann R, Ienco A, Mealli C (2009) Chem Asian J 4:302. doi:10.1002/asia.200800333
22. Mealli C, Hoffmann R, Alvarez S (2009) Submitted for publication
23. von R, Schleyer P, Subramanian G, Dransfeld A (1996) J Am Chem Soc 118:9988. doi:10.1021/ja962036q
24. Burdett JK, Eisenstein O (1995) J Am Chem Soc 117:939
25. Dixon DA, Klier DA, Halgreen TA, Hall JH, Lipscomb WN (1977) J Am Chem Soc 99:7834. doi:10.1021/ja00466a014
26. Graham GD, Marynick DS, Lipscomb WN (1980) J Am Chem Soc 102:2939. doi:10.1021/ja00529a012
27. King RB, Rouvray DH (1977) J Am Chem Soc 99:7834. doi:10.1021/ja00466a014
28. Aihara J (1978) J Am Chem Soc 100:3339. doi:10.1021/ja00479a015
29. Jemmis ED, Subramanian GJ (1994) J Phys Chem 98:9222. doi:10.1021/j100088a022
30. Jemmis ED, Jayasree EG (2003) Acc Chem Res 36:816. doi:10.1021/ar0300266
31. von R Schleyer P, Najafian K (1998) Inorg Chem 37:3454. doi:10.1021/ic980110v
32. Sahin Y, Präsang C, Hofmann M, Geiuseler G, Massa W, Berndt A (2005) Angew Chem Int Ed 44:1643. doi:10.1002/anie.200462397
33. Antipin M, Boese R, Bläser D, Maulitz A (1997) J Am Chem Soc 119:326. doi:10.1021/ja961884i
34. Mealli C, Costanzo F, Ienco A, Peruzzini M, Perez-Carreño E (1998) Inorg Chim Acta 275:366. doi:10.1016/S0020-1693(97)06066-0
35. Hoffmann R (1982) Angew Chem Int Ed Engl 21:711. doi:10.1002/anie.198207113

36. Phillips AD, Ienco A, Reinhold J, Böttcher H-C, Mealli C (2006) Chem Eur J 12:4691. doi:10.1002/chem.200501071
37. Cecconi F, Ghilardi CA, Midollini S, Orlandini A (1991) Z Naturforsch B 46:1161
38. Cecconi F, Ghilardi CA, Midollini S, Orlandini A, Vacca A, Ramírez JA (1990) J Chem Soc Dalton Trans 773
39. Fenske D, Fleischer H, Krautscheid H (1990) Z Naturforsch B 45:127
40. Ghilardi CA, Midollini S, Orlandini A, Scapacci G (1992) J Chem Soc Dalton Trans 2909
41. Haiduc I, Semeniuc RF, Campian M, Kravtsov VC, Simonov YA (2003) Polyhedron 22:2895
42. Matsumoto K, Saiga N, Tanaka S, Ooi S (1991) J Chem Soc Dalton Trans 1265
43. Vicic DA, Jones WD (1999) J Am Chem Soc 121:7606
44. Galli D, Garlaschelli L, Ciani G, Fumagalli A, Martinengo S, Sironi A (1984) J Chem Soc 55
45. Della Pergola R, Garlaschelli L, Martinengro S, Demartin F, Manassero M, Sansoni M (1986) J Chem Soc Dalton Trans 2463. doi:10.1039/dt9860002463
46. Casado M, Perez-Torrente JJ, Ciriano MA, Edwards AJ, Lahoz FJ, Oro LA (1999) Organometallics 18:5299. doi:10.1021/om990623p
47. Fang Z-G, Hor TSA, Mok KF, Ng S-C, Liu L-K, Wen Y-S (1993) Organometallics 12:1009. doi:10.1021/om00028a010
48. Yao W-R, Guo D-S, Liu ZH, Zhang Q-F (2003) J Mol Struct 657:165. doi:10.1016/S0022-2860(03)00415-0
49. Huang K-C, Tsai Y-C, Lee G-H, Peng S-M, Shieh M (1997) Inorg Chem 36:4421. doi:10.1021/ic961482b
50. Seidel R, Schnautz B, Henkel G (1996) Angew Chem Int Ed Engl 35:1710. doi:10.1002/anie.199617101
51. Zhuang B, Chen J, He L, Chen J, Zhou Z, Wu K (2004) J Organomet Chem 689:2674. doi:10.1016/j.jorganchem.2004.05.036
52. Pulliam CR, Thoden JB, Stacy AM, Spencer B, Englert MH, Dahl LF (1991) J Am Chem Soc 113:7398. doi:10.1021/ja00019a041
53. Nishioka T, Isobe K (1994) Chem Lett 1661. doi:10.1246/cl.1994.1661
54. Zimmermann C, Anson CE, Eckermann AL, Wunder M, Fischer G, Keilhauer I, Herrling E, Pilawa B, Hampe O, Weigend F, Dehnen S (2004) Inorg Chem 43:4595. doi:10.1021/ic034876t
55. North TE, Thoden JB, Spencer B, Dahl LF (1993) Organometallics 12:1299. doi:10.1021/om00028a053
56. Carrasco R, Aullòn G, Alvarez S (2009) Chem Eur J 15:536. doi:10.1002/chem.200800914
57. Wiberg KB, Walker FH (1982) J Am Chem Soc 104:5239. doi:10.1021/ja00383a046
58. Nied D, Klopper WF, Breher A (2009) Angew Chem Int Ed 47:2864
59. Mealli C, Ienco A (to be published)
60. Rives AB, You X-Z, Fenske RF (1982) Inorg Chem 21:2286. doi:10.1021/ic00136a032
61. Maj JJ, Rae AD, Dahl LF (1982) J Am Chem Soc 104:3054. doi:10.1021/ja00375a019
62. Dehnen S (2005) Z Anorg Allg Chem 631:604. doi:10.1002/zaac.200400512
63. Zimmermann C, Anson CE, Dehnen S (2007) J Cluster Sci 18:618. doi:10.1007/s10876-007-0130-0
64. Frisch MJ et al (2004) Gaussian 03, revision C.02. Gaussian Inc., Wallingford, CT
65. Becke AD (1993) J Chem Phys 98:5648. doi:10.1063/1.464913
66. Lee C, Yang W, Parr R (1998) Phys Rev B 37:785. doi:10.1103/PhysRevB.37.785
67. Dolg M, Stoll H, Preuss H, Pitzer RM (1993) J Phys Chem 97:5852. doi:10.1021/j100124a012
68. Hariharan PC, Pople JA (1973) Theor Chim Acta 28:213. doi:10.1007/BF00533485